Carbon 150 (2019) 153–167

Contents lists available at ScienceDirect

Carbon

journal homepage: www.elsevier.com/locate/carbon

On the effect of electric field application during the curing process on the electrical conductivity of single-walled carbon nanotubes–epoxy composites

M.V.C. Morais [a, *], A.I. Oliva-Avilés [b], M.A.S. Matos [c], V.L. Tagarielli [c], S.T. Pinho [c], C. Hübner [a], F. Henning [a]

[a] Polymer Engineering Department, Fraunhofer Institut für Chemische Technologie (ICT), Joseph-von-Fraunhofer-Straße 7, Pfinztal, 76327, Germany
[b] División de Ingeniería y Ciencias Exactas, Universidad Anáhuac Mayab, Carretera Mérida-Progreso Km. 15.5 AP 96 Cordemex, 97310, Mérida, Yucatán, Mexico
[c] Department of Aeronautics, Imperial College London, London, SW7 2AZ, United Kingdom

ARTICLE INFO

Article history:
Received 31 December 2018
Received in revised form
20 April 2019
Accepted 23 April 2019
Available online 27 April 2019

ABSTRACT

Single-walled carbon nanotube (SWCNT)/epoxy composites were cured under external electric fields and the influence of the processing parameters (electric field magnitude and frequency, SWCNT concentration and curing temperature) on the electrical response of the system was evaluated. A mold for the electric field application was designed and manufactured, allowing *in situ* measurements of the electrical resistivity of the composite, during and after the curing process. The resulting electrical properties revealed a strong dependence on the processing parameters. By rising the curing temperature, the solid bulk resistivity was decreased by one order of magnitude. Further reduction was observed with electric fields, up to an additional order of magnitude. Such improvements can be related with the decrease in viscosity and improvement of interconnected-nanotube paths within the polymer matrix. The effect of the electric field on the rotation and interconnection of the SWCNTs was investigated using a classical mechanics model based on the dielectrophoretic theory for the liquid state. The influence of inter-nanotube distances on the bulk electrical properties was calculated at different particle concentrations, using finite element models of the microstructure. This processing technique presents promising results for enhancing the electrical conductivity of polymer composites with carbon-based nanoparticles.

1. Introduction

The dispersion of electrically conductive nanoparticles, such as carbon nanotubes (CNTs), in a polymer matrix enables the production of an interesting class of materials in view of commercial applications: electrically conductive polymeric composites. Unlike metals, which tend to have a defined conductivity depending on their elemental properties (aluminum, gold, copper and silver have a conductivity around $3.8 - 6.3 \times 10^5$ S/cm [1,2]), conductive composites allow exploring a wide range of conductivities, from insulator to almost metallic behavior [3]. Adding this electrical-related functionality to the other properties of the polymer matrix, together with versatile processing technologies, may enable many promising opportunities for the replacement of metals in applications such as heating elements, electromagnetic interference shielding, lightweight construction and battery technologies, given the corrosion resistance of some polymers (e.g. in bipolar plates for redox-flow batteries) [4–6]. Furthermore, their electrical response to external stimulus (e.g. mechanical, thermal, chemical) enables several kinds of sensing applications, such as strain and damage for health monitoring systems, as well as temperature, gas, or biodegradation, amongst others [3,7–9]. However, tuning the electrical conductivity of the final conductive composite is not trivial. According to percolation theory for electrical problems [10–12], for each system there is a minimum particle concentration required, the percolation threshold, to attain a conductive particle network that enables the flow of electrons. Further particle addition often brings a smaller improvement compared to the conductivity increase of several orders of magnitude that occurs around this threshold.

* Corresponding author.
E-mail address: manuel.morais@ict.fraunhofer.de (M.V.C. Morais).

https://doi.org/10.1016/j.carbon.2019.04.087
0008-6223/

Numerous reports of percolation thresholds for different polymer-particle matrix systems can be found in the literature [11,12]. This value mainly depends on the particle shape and properties as well as on the matrix and the selected processing technique. Many variables play a role on the final particle network structure: the original state of agglomeration and geometry of the particles, viscosity of the matrix, processing parameters such as temperature and shear stresses undergone by the material, etc. [11–15]. Understanding these phenomena, the role of the different processing parameters on the resultant nanoparticle network structure, and how this structure influences the final effective properties of the composites, is therefore of paramount importance for exploring their full potential and enabling their industrial widespread use.

One convenient approach for influencing nanoparticles dispersed in liquid medium is the use of electric fields; inducing polarization of the particles leads to dipole interactions between them in a phenomenon governed by the dielectrophoretic theory. Since the pioneer reports of Yamamoto et al. [16,17], the use of electric fields for CNT manipulation has been frequently addressed in literature [18–22]. However, up until the work of Martin et al. [23] in 2005, electric fields had only been applied to dispersions of nanotubes in different solvents such as ethanol and dimethylformamide. Following their experiments, dielectrophoresis (DEP) has been reported to influence the network structure of CNTs in different polymer matrices and hence the electrical properties [24–31]. A comprehensive review by Remillard et al. [32] compares different attempts in terms of the many parameters that play a role in this phenomenon such as: electrode material and spacing, the CNT type, the liquid medium, the particle concentration, the electric field voltage and frequency, and the duration of exposure to the electric field. These results not only demonstrate the potential of DEP for the manipulation of carbon nanotubes within a low viscosity polymeric matrix, but also point out to the challenging complexity of the process. Clear understanding of the dependency of this process on the electric field frequency, as well as its limitations in terms of range of particle concentration where it can be applied (e.g. effectiveness below and above percolation) are questions which remain to be addressed.

The present research focuses on the improvement of the electrical conductivity in a system of epoxy and commercial single-walled carbon nanotubes (SWCNT). Influence of the electric field parameters (strength and frequency), particle concentration, and curing temperature of the epoxy matrix were investigated. In order to further understand the observed decrease of the electrical resistivity of the composites due to the electric field, its influence on the CNT rotation and interconnection was studied by modeling the interaction between two SWCNTs using classical mechanics and DEP theory. Finally, the impact of the distance between adjacent CNTs in the bulk on the electrical properties was explored using finite element (FE) analysis for a variety of particle concentrations, revealing resistivity changes compatible with the experimental observations.

2. Methods and equipment

2.1. Preparation of the SWCNT/epoxy liquid solution

Epoxy resin Epikote MGS RIMR426 (viscosity of 500 – 900 mPa•s at 25 °C) and curing agent Epikure RIHMH433 were obtained from Lange-Ritter GmbH. Pristine SWCNTs TUBALL™ in powder form provided by OCSiAl were used (diameter of 1.6 ± 0.4 nm and length >5 μm [33]).

A three-roll mill (Exakt 80E, Germany), with 200 mm length and 80 mm diameter rolls made of chemically neutral silicon carbide, throughput capacity of 20 – 20000 cm^3/h and a minimum gap achievable between rolls of 5 μm, was employed to mechanically disperse the SWCNTs in the epoxy resin. As depicted in Fig. 1, the mill is composed of three rolls coupled together to operate at different speeds – the set speed is given for the apron roll, while the center and feed rolls follow with 3 and 9 times slower, respectively. The suspension is poured on the feed roll, that forces it to pass through the first gap (set to 15 μm) while undergoing shear forces generated by the rotation at different speed of the center roll. The material then goes through a second smaller gap (set to 5 μm) and is finally collected by a sharp blade in contact with the apron roll, ending a cyclic process hereby called “pass”. For this study, the speed of the apron roll was set to 180 rpm and seven mixing passes were performed on the resin. The state of dispersion of the SWCNTs within the epoxy liquid solution using the three-roll mill technique has been previously explored [14,15] and the parameters here selected were chosen from preliminary experiments until a stable electrical response (associated with a stable state of SWCNT dispersion) of the solid samples was achieved. The SWCNT weight concentrations (ϕ) of 0.001, 0.005, 0.01 and 0.1wt.% were investigated.

2.2. Fabrication and characterization of SWCNT/epoxy composites

A mold made from silicone containing a heating block between two sample gaps (Fig. 2b) was used for the application of electric fields during the curing process of the composites. Two SWCNT/epoxy specimens (22.5 mm × 12 mm × 1.65 mm) were produced simultaneously under the same curing conditions but only one of them was under the influence of the electric field by connecting the electrodes to the voltage source (the other was used as a reference, i.e. without electric field). Gold-coated copper rectangular pieces with dimensions 24 mm × 14 mm were used as electrodes for the electric field application. The electrodes were covered with silver paint as an electrically conductive mold release agent. The effect of the electric field on the electrical properties of the SWCNTs/epoxy nanocomposites was investigated by measuring their electrical resistance by means of two different techniques: with a multimeter after the curing process (*ex situ*); and by tracking the direct current (DC) flowing through the specimen during the application of the alternate current (AC) electric field (*in situ*).

The following procedure was executed for each experiment: 2 g of epoxy resin filled with SWCNTs (previously dispersed in the three-roll mill) were hand-mixed with 0.56 g curing agent (weight ratio 100:26), as prescribed by the manufacturer, and fed into the two spaces between the electrodes (Fig. 2a) with a volumetric pipette. The absence of bubble formation was visually confirmed and a preliminary experimental study revealed that degasification prior to curing does not significantly affect the final conductivity. The electrode pair of one of the samples (the test sample) was then connected to the voltage supply. The desired electric field parameters were set (strength and frequency) and, as soon as the power supply was on, the temperature was set on the heating block (1 min to reach). The effect of curing temperature on the final resistivity of the composites was investigated by curing at room temperature (RT), 80 °C and 100 °C (temperature set in the heating block and measured with a thermocouple). The curing time was dependent on the temperature; approximately 2 h for RT and less than 10 min for 80 °C and 100 °C (discussed later). After the cure, the voltage was turned off and once the samples had cooled down to room temperature, the *ex situ* electrical resistance of both (test and reference) was measured by attaching a multimeter to the two respective electrode pairs.

Furthermore, to investigate the dynamics of the CNT interconnection and network formation process during the curing process,

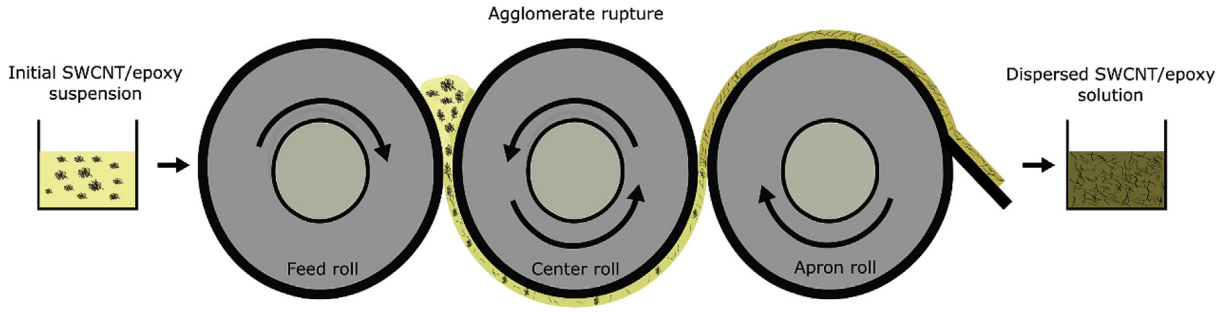

Fig. 1. Dispersion of the SWCNTs in the three-roll mill. SWCNT/epoxy suspension is poured between the feed and center rolls, passes through the two adjustable gaps and is collected on the apron roll. (A colour version of this figure can be viewed online.)

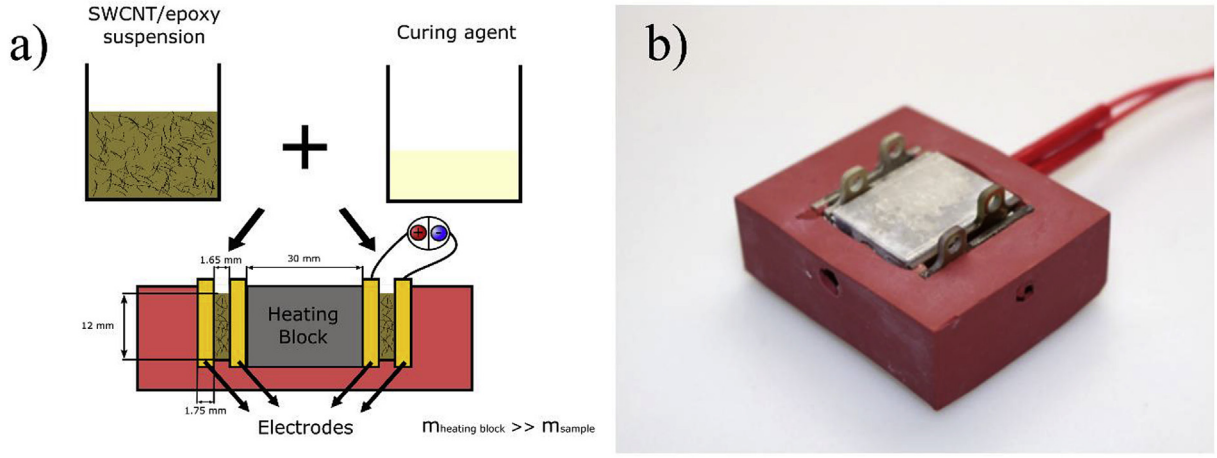

Fig. 2. For sample production: a) the SWCNT/epoxy suspension was mixed with the curing agent and then fed into the two sample forms, b) silicone mold used for curing samples under an electric field. (A colour version of this figure can be viewed online.)

in situ resistance measurements were performed during all experiments. A suitable approach to track the DC resistivity was to add a 1 V_{DC} offset to the AC voltage applied and measure the respective DC current with a multimeter connected in series (A in Fig. 3a). An additional multimeter connected in parallel (V in Fig. 3a) recorded the DC offset for confirmation. Both multimeters filter the AC components of the voltage and current when they are measuring in DC mode.

The *in situ* measurements resulted in a time vector of the DC voltage (1 V) and the DC current. Using Ohm's law $U = R \times I$, along with the relation for the volume resistivity $\rho = R \times A/L$, where U is the voltage, R the resistance, I the current, ρ the volume resistivity, A the area of the sample and l the thickness, the DC resistivity was then computed. Four samples were tested for each experimental setting and the average value was calculated. The error bars in the plots correspond to the minimum and maximum values. The rheological properties of the epoxy and SWCNT/epoxy suspensions, as well as of the reacting system with curing agent, were investigated at 20 °C (RT), 80 °C and 100 °C using an MCR 501 rheometer (Anton Paar, Austria). The complex viscosity was measured by

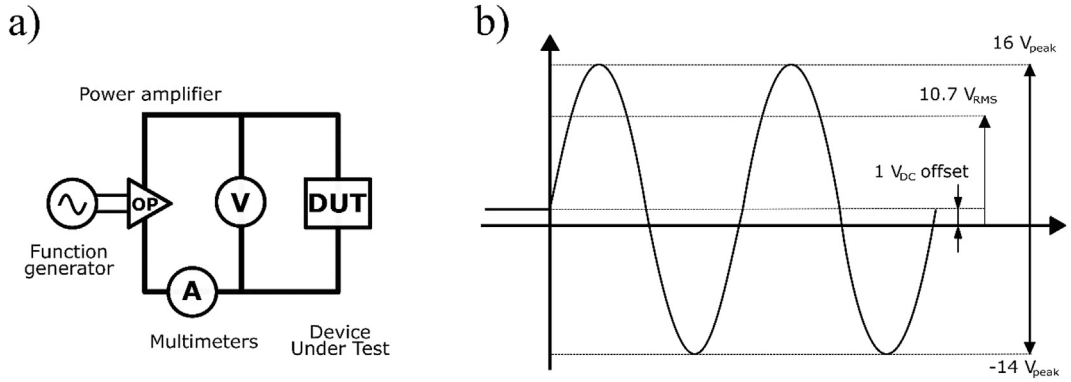

Fig. 3. Schematic of: a) the electrical setup, and b) the respective AC signal used for the experiment signal: the DC offset of 1 V added to the 30 V peak-to-peak sinus, allowing measurement of the resistance improvement *in situ*.

operating the rheometer in oscillatory shear mode with parallel plate configuration (25 mm diameter cell). The composite samples were examined using a Zeiss Supra 55-VP (Carl Zeiss, Germany) Scanning Electron Microscope (SEM) equipped with an in-Lens detector and operating at 3 kV. Specimens were gold-sputtered using a Cressington 208HR high-resolution sputter coater before the SEM measurements.

2.3. Electric field application and in situ measurement of the electrical resistivity

To generate the electric field, a voltage of up to 30 $V_{peak-to-peak}$ and frequency of up to 10 MHz was applied, with a DC offset of 1 *V* to perform *in situ* resistance measurements, as illustrated in Fig. 3b. For each experiment, the wave (input) signal was defined in the function generator (Agilent 33250A) by setting the voltage and frequency, which was then connected to the high frequency power amplifier (Tabor 9260), which increases the voltage input by a factor of 10 (up to 36 $V_{peak-to-peak}$) and provides a current of up to 1 A. In the present case, most of the experiments were performed with 3 $V_{peak-to-peak}$ selected on the function generator, meaning 30 $V_{peak-to-peak}$ output voltage at the power amplifier. This corresponds to a peak voltage of ±15 V_P (measured with a Tektronix MSO 2014 Oscilloscope) and effective voltage of 10.6 V_{RMS}. For a meaningful corresponding DC voltage (Delta Elektronika ES 030–10), 10.6 V_{DC} was used for the direct current investigations. Adding 1 V_{DC} to the AC signal (Fig. 3b) only changes the total voltage by 1% (to 10.7 V_{RMS}), which represents a negligible difference. This DC voltage and the DC current were measured with two Metrix MTX 3283B Multimeters (V and A in Fig. 3a, resp.) In addition to the electrical setup, the distance between the electrodes plays a crucial role in the experiments since it defines the electric field strength according to $E = U/d$, where U is voltage and d distance. For an average thickness of 1.65 mm and a voltage of 10.7 V_{RMS}, the effective electric field over the samples is E = 6.5 V_{RMS}/mm. Voltages higher than 30 $V_{peak-to-peak}$ (maximum of the amplifier) and frequencies above 10 MHz (to prevent undesired high frequency-related inductivity effects occurring after this frequency) were not tested.

2.4. Dielectrophoretic model of interacting SWCNTs immersed in a fluid

To elucidate the role of the main experimental parameters involved in the curing process when the electric field is applied, an analytical simplified approach based on classic mechanics and on the dielectrophoretic theory is used [34,35]. According to the DEP theory, when an electric field is applied to a system of particles immersed in a fluid, the charge distribution is rearranged at the interphase of the particle/medium system due to their different dielectric properties (electrical conductivity and permittivity) [36,37]. Furthermore, the effective dipole moment approach [36,37] considers that such a rearrangement of charge induces a dipole moment on the CNTs, which would interact with the electric field causing the rotation (alignment) and translation of CNTs. As such, the model conceives the CNTs as electrical dipoles, with positive and negative induced charges at their opposite ends, see Fig. 4. The model considers two metallic CNTs (CNT-1 and CNT-2) as straight and rigid prolate ellipsoids in a one-dimensional framework, with major semi axis a, centers of charge in coordinates x_1 and x_2 and deviation angles of θ_1 and θ_2, being these the angles comprised between the CNT axis and the direction of the electric field (E) (horizontal in Fig. 4). It is important to mention that the assumption of CNTs as straight and rigid is an idealization; CNTs are wavy and generally entangled. However, such an assumption

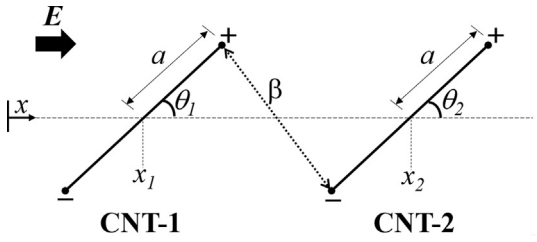

Fig. 4. Schematic of the CNTs and illustration of variables of the DEP model.

allows the development of a simplified model exploring coupled rotational and translational motion which helps to understand the CNT response under AC electric fields and therefore the formation of interconnected conducting networks [34,35]. The model also considers a CNT/medium interphase layer (not illustrated in Fig. 4) which captures the effect of the electric field frequency (f) on the magnitude of the induced dipole on the CNTs [34].

To evaluate the CNT rotation and translational motion, a set of coupled nonlinear differential equations based on Newton's Second Law are considered for each case. For the rotational motion, the governing motion equation for each CNT is given by,

$$I\frac{d^2\theta}{dt^2} + T_{DEP} + T_{fr} + T_{coup} = 0 \tag{1}$$

In Eq. (1), $I = m(a^2 + b^2)/5$ where $m = d_{CNT}V$ is the mass of the CNTs, d_{CNT} is the CNT density, V is the volume ($V = 4\pi ab^2/3$), and a and b are the major and minor CNT semi axes, respectively. The second term in Eq. (1), T_{DEP}, corresponds to the DEP torque exerted by the CNT due to the presence of an electric field and is given by the expression,

$$T_{DEP} = \frac{1}{4}V_{\varepsilon_m}E^2\mathrm{Re}[\alpha^*]\sin 2\,\theta \tag{2a}$$

$$\alpha^* = \frac{\left(\varepsilon^*_{eq} - \varepsilon^*_m\right)^2}{\left[\varepsilon^*_m + \left(\varepsilon^*_{eq} - \varepsilon^*_m\right)L\right]\left(\varepsilon^*_{eq} + \varepsilon^*_m\right)} \tag{2b}$$

$$\varepsilon^*_{eq} = \varepsilon^*_{lay}\left[\frac{\varepsilon^*_{CNT} + \frac{\delta}{2a}\left(\varepsilon^*_{CNT} - \varepsilon^*_{lay}\right)}{\varepsilon^*_{lay} + \frac{\delta}{2a}\left(\varepsilon^*_{CNT} - \varepsilon^*_{lay}\right)}\right] \tag{2c}$$

$$\varepsilon^* = \varepsilon - j\frac{\sigma}{2\pi f} \tag{2d}$$

where E is the electric field magnitude, δ is the thickness of the interphase layer, $L = \left[\ln\left(\frac{2a}{b}\right) - 1\right] \Big/ \left(\frac{a}{b}\right)^2$ is the CNT longitudinal depolarization factor [34,37], ε is the permittivity, σ the electrical conductivity and subscripts “CNT”, “m” and “lay” stand for carbon nanotube, surrounding medium and interphase layer, respectively. From Eq. (2b), it can be observed that α^* depends on the electric field frequency f, and the real part (Re) of α^* impacts on the magnitude of T_{DEP}. Readers are referred to Refs. [34,35] to find more detailed explanations and rationale regarding the expression of T_{DEP}. In Eq. (1) T_{fr} refers to the frictional (viscous) torque and T_{coup} represents the torque exerted by the CNT due to the presence of the other CNT. Expressions for T_{fr} and T_{coup} terms in Eq. (1) can be found elsewhere [35]. Initially, the CNTs were considered misaligned in respect to the electric field, with initial angles set to 89°

(instead of 90°) to avoid numerical issues during the computational solution process due to the nonlinearity of the equations. The initial angular velocity was set to zero. The evolution of the rotational angles of the CNTs is obtained by solving Eq. (1) numerically.

Using a similar rationale, the governing equation for the translational motion is given by,

$$m\frac{d^2x}{dt^2} + F_{fr} + F_{coup} + F_{rep} = 0 \tag{3}$$

where F_{fr} and F_{coup} refer to the frictional and coupling forces exerted by each CNT, see Ref. [35]. F_{rep} in Eq. (3) refers to a short-range repulsive force that decays quickly with the CNT-to-CNT separation distance (β, see Fig. 4), which is incorporated to the model to prevent the CNT overlapping [35]. By numerically solving Eq. (3) the time evolution of the position of both CNTs' centers of mass, and therefore β, can be computed. The initial positions of CNTs were set in such a way that the horizontal distances between their centers of mass ($x_2 - x_1$ in Fig. 4) was 7 μm, and their initial translational velocity was zero. It is important to note that Eqs. (1) and (3) are coupled by the direct dependence of T_{coup} on F_{coup} terms [36]. Also, it is important to point out that both governing equations are dependent on the CNTs longitudes ($L_{CNT} = 2a$), as the positions of the DEP induced charges at the CNTs ends (and therefore the induced forces and torques) are directly correlated to such longitudes. The main outcomes of the DEP model are the evolution of the CNTs deviation angles (θ_1 and θ_2) and the CNT-to-CNT separation distance (β), being the former an indicator of CNT alignment and the latter an indicator of CNT chaining.

Table 1 shows the fixed value parameters used in the model, selected based on the experimental conditions used in this study and previous works [34,35]. It should be noted that a CNT/epoxy curing under electric fields is a complex system with several influencing factors. Viscosity, electric field magnitude and frequency were varied in the model using experimentally used values, and the influence of such changes is evaluated in the model predictions. The permittivity of the fluid (liquid epoxy) is assumed to be 11, which was measured with dielectric spectroscopy at RT. In general, the permittivity of the resin depends on the temperature but is expected that the moderate increase of the T (up to 100 °C) does not change significantly such a value. Additionally, the very high difference between permittivity of fluid and particle makes the slight changes on the fluid permittivity almost negligible for the effective DEP forces and torques [35,36].

Table 1
Numerical parameters used in this study.

Physical property		Fixed value
CNT	Permittivity, ε_{CNT}	1×10^5 [35]
	Electrical conductivity, σ_{CNT}	1×10^4 S/m [38]
	Density, d_{CNT}	2000 kg/m^3 (est. from [39])
	Major semi-axis, $a = L_{CNT}/2$	2.5 μm [33]
	Minor semi-axis, $b = D_{CNT}/2$	1 nm [33]
	Aspect ratio	2777
Fluid	Permittivity, ε_m	11 [exp, RT]
	Electrical conductivity, σ_m	3×10^{-5} S/m [exp]
	Viscosity, μ	30 and 1500 mPa•s [exp]
CNT/fluid interphase layer	Electrical conductivity, σ_{lay}	1×10^{-4} S/m [35]
	Permittivity, ε_{lay}	1×10^4 [35]
	Thickness, δ	10 nm [35]
Electric field	Magnitude, E	2.1 and 6.5 V/mm [exp]
	Frequency, f	50 HZ and 1 MHz [exp]

2.5. FE modeling of the bulk conductivity of CNT-polymer networks

With the objective of quantifying the effect of the distance between CNTs on the bulk electrical properties of these composite materials, the FE methodology presented in Ref. [40] is here applied. This methodology allows for modeling all the main mechanisms of conductivity in these systems: 1) conductivity of the CNTs, 2) conductivity across CNT-CNT junctions and 3) conductivity of the polymeric matrix. Electrical conductivity is calculated based on simulations of representative volume elements (RVE) where CNTs are randomly distributed in a cubic matrix.

For this approach, the CNTs are described by continuum cylinders with prescribed length L_{CNT} and external diameter D_{CNT}. These are seeded at random locations within the RVE of side L_{RVE}, and at random azimuthal and latitudinal angles. Since the nanotubes are impenetrable, a search for intersections is performed. When an intersection is detected, the respective nanotubes are locally deformed so that the minimum distance that separates them d_{min} is never inferior to the van der Waals equilibrium distance of 0.34 nm [41]. Once the desired volume fraction is reached, geometric periodicity is enforced so that the macroscopic material can be idealized as a periodic repetition of the RVE along all Cartesian directions, as represented in Fig. 5.

The electrical analysis is performed using Abaqus Standard steady-state heat-transfer analysis [42], replacing all thermal properties with the adequate electrical equivalents [43]. The CNTs are modeled by DC1D2 2-noded link heat transfer elements that are embedded in the polymeric matrix, discretized by a regular mesh of DC3D8 8-noded brick elements. The conductivity between adjacent CNTs is modeled with a user element [40] integrated into a Fortran UEL subroutine in Abaqus [44] that reproduces the fluctuation-induced tunneling electron transport [45] using Simmons's generalized formula [46]. The tunnel current density J across the contacting CNTs that are separated by a thin insulating layer of permittivity ε can be expressed as a function of the separation s between them, as

$$J = J_0\left\{\overline{\varphi}e^{-A\sqrt{\overline{\varphi}}} - (\overline{\varphi} + eV)e^{-A\sqrt{\overline{\varphi}+eV}}\right\}$$
$$J_0 = \frac{e}{2\pi h(\Delta s)^2} \text{ and } A = \frac{4\pi\Delta s}{h}\sqrt{2m_e} \tag{4}$$

where the constants e and m_e represent the charge and mass of the electron, respectively, and h is the Planck's constant. $\overline{\varphi}$ is the mean value of the potential barrier, which has two roots at positions s_1 and s_2, with $\Delta s = s_2 - s_1$. For a potential barrier of magnitude φ_0, here taken as the CNT work function, these can be approximated by [46].

$$\overline{\varphi} = \varphi_0 - \left(\frac{eV}{2s}\right)(s_1 + s_2) - \left[\frac{1.15\omega s}{s_2 - s_1}\right]\ln\frac{s_2(s - s_1)}{s_1(s - s_2)}$$

$$s_1 = \frac{1.2\omega s}{\varphi_0} \text{ and } s_2 = \begin{cases} s_1 + s\left[1 - \dfrac{9.2\omega}{3\varphi_0 + 4\omega - 2eV}\right], & eV < \varphi_0 \\ (\varphi_0 - 5.6\omega)\left(\dfrac{s}{eV}\right), & eV \geq \varphi_0 \end{cases}$$

$$\omega = \frac{e^2 \ln 2}{8\pi\,\varepsilon\, s} \tag{5}$$

This effect is here described as an equivalent parallel-plate capacitor of area D_{CNT}^2 and separation s. The element is applied to every contact point between distinct nanotubes within a distance inferior to $d_{cut-off} = 4$ nm. Periodic boundary conditions are

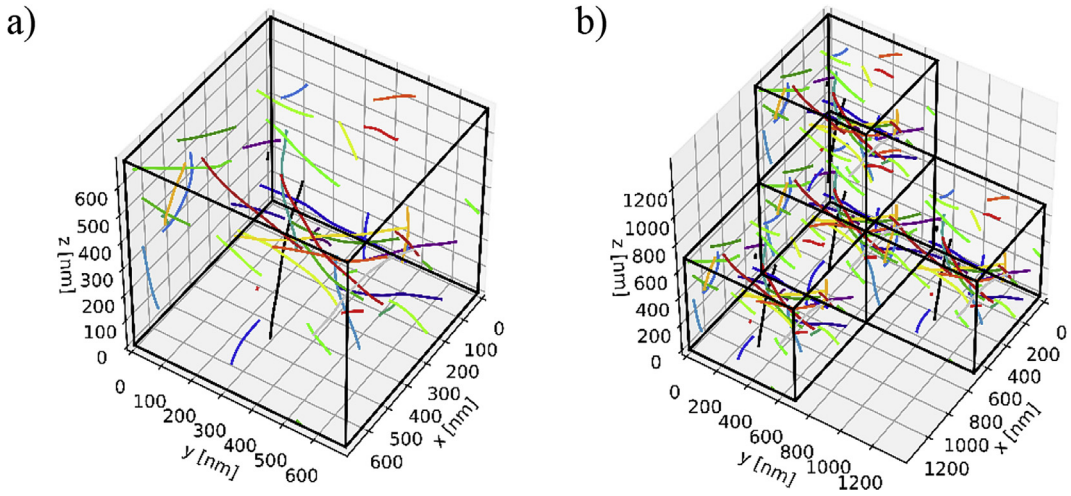

Fig. 5. Example of a) an RVE and b) its periodicity. (A colour version of this figure can be viewed online.)

enforced at every boundary of the RVE and 3 load steps are created, each representing a homogenized electric field along each of the 3 Cartesian directions, allowing the retrieval of the conductivity all directions (which should tend to the same number for an isotropic dispersion).

3. Results

Electric fields were applied to SWCNT/epoxy composites during curing according to the methodology described in Section 2. In this section, the effects of varying the electric field strength, frequency, curing temperature and SWCNT concentration are introduced. *Ex situ* and *in situ* measurements are presented in Sections 3.1 and 3.2, respectively. Section 3.3 contains the results of rheological measurements of epoxy resins with different SWCNT concentrations and cured at different temperatures for 0.01 wt%. Section 3.4 presents the results of modeling the interactions between two SWCNTs in an electric field using classical mechanics and DEP theory (described in Section 2.4). Furthermore, Section 3.5 explores the impact of the contact distance between adjacent CTNs influenced by these interactions on the composite bulk electrical properties using FE simulations (introduced in Section 2.5) of the CNT networks. Finally, Section 4 presents a discussion about the experimental observations and the modeling results.

3.1. Electrical resistivity of solid composites fabricated under electric fields

Fig. 6 showcases the impact of varying the electric field strength during curing on the final electrical resistivity of SWCNT/epoxy composites at 0.01 wt.%, obtained by varying the applied voltage, at a frequency of 10 MHz. A clear effect of the field strength on this electrical property is verified from the comparison of the three steps. Reduced electrical resistivity of the solid nanocomposites was observed with increased field strength, being understood in terms of the induced electrical force on the nanoparticles (which is directly proportional to the square of the field strength, see Eq. (2a)).

Fig. 6 also suggests a decrease in the resistivity values dispersion for higher field strength as the difference between maximum and minimum values decreases notoriously (see error bars). This represents another indication of the importance of this parameter for the formation of more stable and effective CNT conductive networks within the polymer, thus improving reproducibility of the

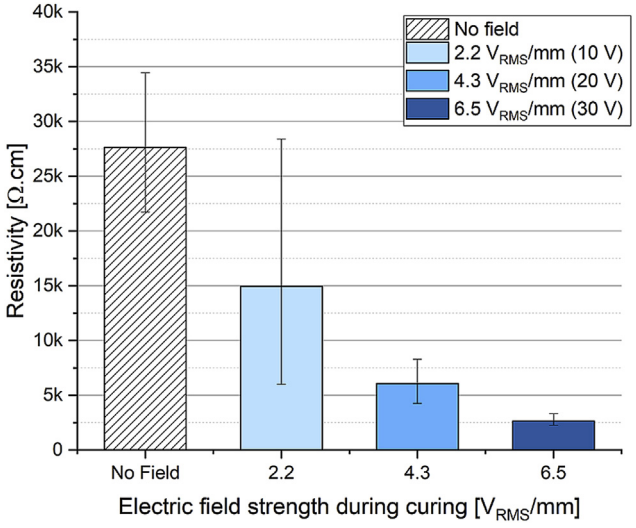

Fig. 6. Impact of electric field strength (@10 MHz) on the final electrical resistivity of epoxy/SWCNTs 0.01 wt.% solid composites cured at a set temperature of 80 °C. (A colour version of this figure can be viewed online.)

results.

In a second stage, the electric field strength was fixed at 6.5 V_{RMS}/mm (corresponding to 30 $V_{peak-to-peak}$) and the frequency was varied to investigate its impact on the through-plane electrical resistivity of the SWCNT/epoxy nanocomposites. Results are depicted in Fig. 7. While the DC field does not show significant changes on the resistivity as compared with the reference case (without electric field), a decrease in resistivity with increased frequency is clearly observed, with a resistivity plateau starting at 50 kHz. A high scatter of data for the reference samples cured without any electric field and the DC ones was observed, in contrast with the stable measurements noticed when AC electric field was used. This decreasing behavior of the scatter might additionally point to an improvement of the carbon nanotube networks that are settled between the electrodes during the process.

To understand the role of the epoxy curing dynamics on the formation of the electrically conductive networks, the curing temperature was varied by changing the set temperature on the heating block in the mold. Samples were cured at room temperature (RT), 80 °C and 100 °C, with final resistivities presented in

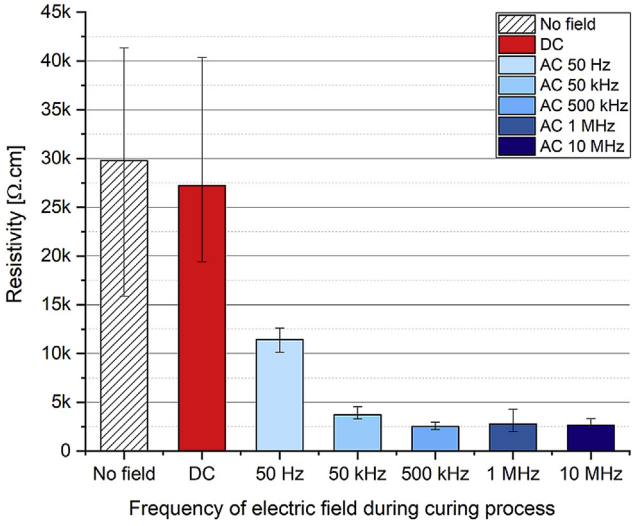

Fig. 7. Impact of frequency of the electric field (6.5 V_{RMS}/mm) on the final electrical resistivity of SWCNT/epoxy 0.01 *wt.%* composites cured at a set temperature of 80 °C. (A colour version of this figure can be viewed online.)

Fig. 8, for an electric field with amplitude 6.5 V_{RMS}/mm and frequency 10 MHz. For the experiments without application of electric field, increasing the curing temperature from RT to 100 °C shows a remarkable decrease in resistivity, by almost an order of magnitude, falling from more than 100 $k\Omega$·cm to almost 20 $k\Omega$·cm. The resistivity was further reduced when cured in the presence of an AC field, as described in Fig. 8.

Lastly, to evaluate the effect of the nanotube concentration on the resistivity, samples with CNT concentrations (ϕ) of 0.001, 0.005, 0.01 and 0.1 wt.% were fabricated at 80 °C, with and without AC electric field application (Fig. 9). For the lowest amount of SWCNTs, 0.001 wt.%, the *ex situ* electrical resistivity was too high to be measured by the multimeter in resistance mode (limited to 50 $M\Omega$) and hence no values are presented. This means that the percolation concentration lies between 0.001 wt% and 0.005 wt% for samples cured at 80 °C. The same trend was found for specimens cured at room temperature, with SWCNT/epoxy 0.005 wt% also being conductive.

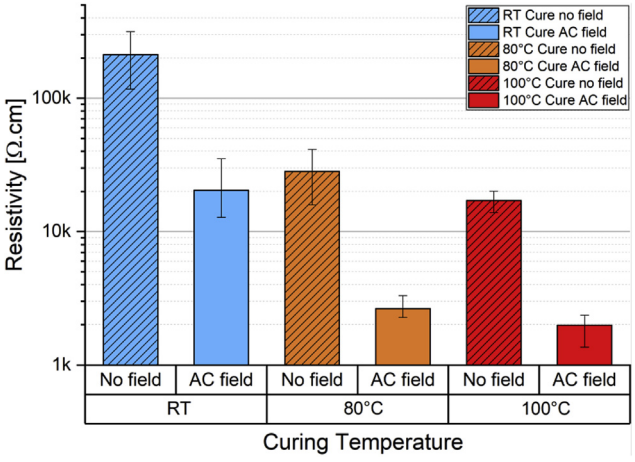

Fig. 8. Impact of AC electric field (6.5 V_{RMS}/mm @10 MHz) during curing at different temperatures on the through-plane electrical resistivity of epoxy/SWCNTs 0.01 wt.% nanocomposites. (A colour version of this figure can be viewed online.)

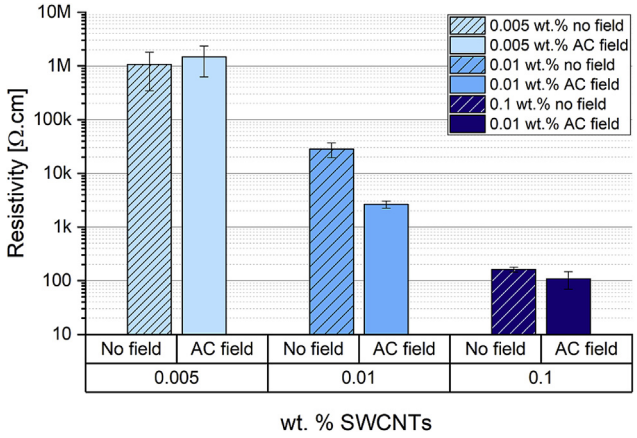

Fig. 9. Impact of AC electric field (6.5 V_{RMS}/mm @10 MHz) during curing (at a set temperature of 80 °C) of epoxy/SWNTs with different concentrations on the through-plane electrical resistivity. (A colour version of this figure can be viewed online.)

Fig. 9 shows that the electrical resistivity decreases with increased CNT concentration. The effect of the electric field application becomes significant at 0.01 wt.% and above; no differences are noticed for the composite at the lowest (0.005 wt.%) concentration.

From these results it can be inferred that the possibility of decreasing the electrical resistivity for this SWCNT/epoxy nanocomposite system is limited to CNT concentrations of 0.01 wt.% and above. Moreover, this improvement seems to be less effective for 0.1 wt.%, what could be caused by the significant increase in viscosity (see rheology measurements in Section 3.3), hindering the mobility of the carbon nanotubes. This is further discussed in Section 4.

3.2. Dynamic evolution of electrical resistivity for SWCNT/epoxy liquid systems

To calculate the *in situ* DC resistivity during the electric field treatment, the DC current flowing through the samples due to the 1 V_{DC} offset added to the AC field was measured, as explained in Sections 2.2 and 2.3. The measured electrical current was in different ranges according to the SWCNT concentration: 0 – 700 nA for 0.001wt.%; 20 nA – 6 μA for 0.005wt.%; 30 μA – 3 mA for 0.01wt.% and 7 mA – 180 mA for 0.1wt.%.

The *in situ* evolution of the DC resistivity with elapsed time for the samples produced with different concentrations is represented in Fig. 10. Despite the fact that no *ex situ* resistivity values could be obtained from the composite samples with 0.001 wt.%, *in situ* measurements are not only able to provide additional information for this concentration, but also for the pure epoxy resin, as presented in Fig. 10. The evolution of the resistivity with the curing time is able to provide valuable insight into the curing dynamics of the resin, showing a similar behavior with four different phases. Furthermore, this indicates that the slight increase in resistivity after the minimum – pointed out as phase 3 – must be related to the crosslinking process, since it also happens for the pure resin (in this case related to the reduction in the concentration of unreacted amine and epoxy molecules, potential charge carriers [23]).

It is important to notice that two processes are taking place simultaneously, affecting the resistivity measurements. On one hand there is the crosslinking reaction of the epoxy resin, whose dynamics might affect the nanotube dispersion state and hence the electrical resistivity. On the other hand, there is the effect of the electric field which affect the nanotube distribution. In Fig. 11 it is

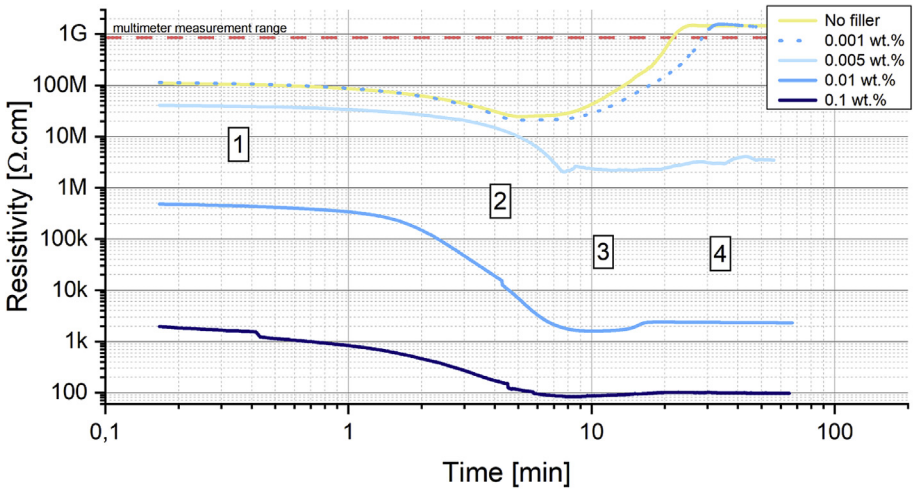

Fig. 10. *In situ* resistivity measurements during the curing process under an AC electric field (6.5 V/mm @10 MHz) for different SWCNT/epoxy concentrations cured at a set temperature of 80°C. (A colour version of this figure can be viewed online.)

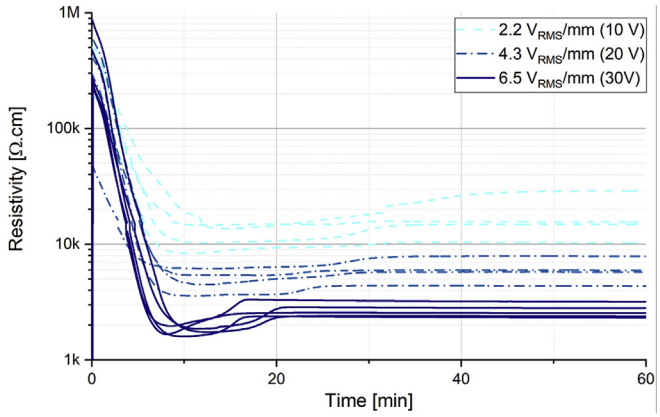

Fig. 11. Impact of electric field strength on the *in situ* resistivity during the curing of epoxy/SWCNTs 0.01 wt.%. Frequency was set to 10 MHz and curing temperature was set to 80 °C. (A colour version of this figure can be viewed online.)

possible to observe the influence of the electric field strength on the final resistivity values, which are in agreement with the *ex situ* measurements (Fig. 6).

Additionally, the *in situ* curves provide valuable information about the dynamics of the processes occurring during the experiments. For all the investigated electric field strengths, an initial significant decrease on the resistivity was observed, around the first 7–9 min, followed by a slight progressive increase until reaching a stationary value. This slight increase in resistivity may be correlated with the curing process; the reduction in the concentration of unreacted amine and epoxy molecules (potential charge carriers) decreases the ionic conductivity [23]. Interestingly, the time that the resistivity takes to stabilize around its final value decreases with the field strength. This behavior might be an indication of a faster epoxy-amine reaction completion for the case of 6.5 V_{RMS}/mm, as opposed to a longer network consolidation for 4.3 and 2.2 V_{RMS}/mm, possibly induced by the higher electrical currents flowing through the sample and resulting known electrothermal mechanisms such as the Joule effect [47].

Fig. 12 presents the impact of curing temperature on *in situ* resistivity measurements, where time is plotted with a logarithmic scale in the horizontal axis. The first valuable remark is the

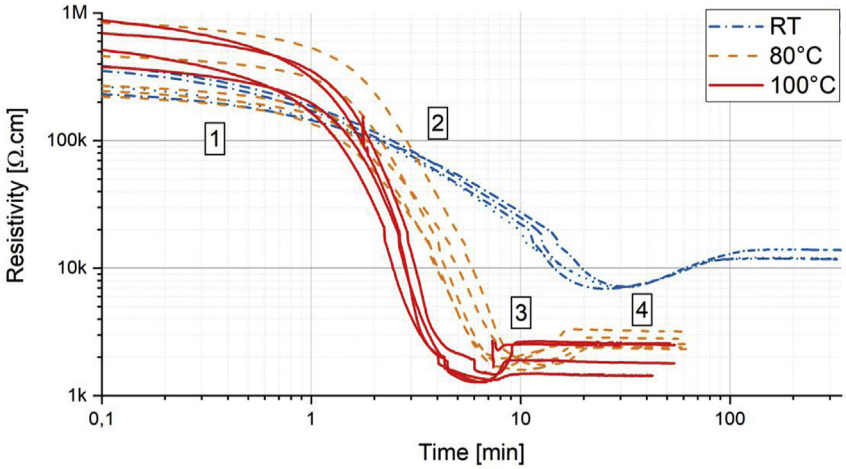

Fig. 12. Impact of AC electric field (6.5 V/mm @10 MHz) at different (set) curing temperatures on the *in situ* electrical resistivity of SWCNT/epoxy 0.01 wt.% nanocomposites. 1 to 4 indicate the different stages for 80 °C curing (orange). (A colour version of this figure can be viewed online.)

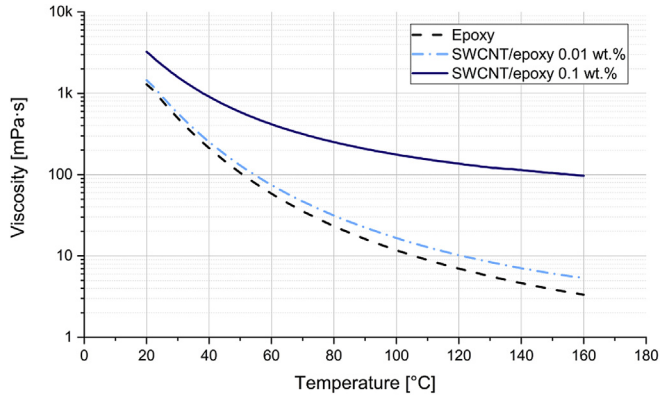

Fig. 13. Viscosity measurements of the pristine epoxy and SWCNT/epoxy composite resin with temperature (without curing agent). (A colour version of this figure can be viewed online.)

agreement between the final resistivity values and the *ex situ* measurements in Fig. 8. It is also possible to clearly distinguish 4 different stages (see Fig. 12) that the process undergoes while curing at 80 °C (orange curves): 1) an initial gradual decrease in the first minute; 2) a pronounced fall until a minimum is reached around 10 min; 3) an additional increase lasting up to 10 min; and 4) a final plateau corresponding to the final *ex situ* resistivity. This non-monotonic behavior of resistivity is likely related to the final stage of the epoxy cross-linking process and its associated shrinkage, distorting the SWCNT network [23]. The curing temperature seems to strongly influence the duration, the slope and resistivity interval of each of the 4 phases and, overall, there is good agreement between the four experiments for each temperature setting. For this epoxy system, higher temperatures favor states of lower viscosity, which might allow an improved mobility of the CNTs and hence more effective action of the electric field on the induced assembly.

3.3. Rheology measurements

Fig. 13 depicts the viscosity measurements of the epoxy and composite resin as a function of temperature. As expected, a strong dependency of viscosity on temperature was found – for pure epoxy it decreased two orders of magnitude, from around 1Pa · s at 20 °C to 10 mPa·s at 100 °C. The addition of only 0.01 wt.% SWCNTs leads to a slight increase of viscosity of the composite resin, whereas for 0.1 wt.% there is a remarkable difference (one order of magnitude higher at 100 °C). Given the fact that the viscosity of a fluid provides an indication of its mobility and that of the particles immersed in it, these results might explain the tendencies found when curing the materials at different temperatures (Figs. 8 and 12). Higher temperatures lead to a lower viscosity and hence increased mobility of the SWCNTs, promoting reduced CNT-to-CNT separation distances and CNT chaining and therefore lower resistivity.

The viscosity of the SWCNT/epoxy system (with the curing agent) was evaluated. The complex viscosity (η^*) of the reacting system was investigated for the three different temperatures (20 °C, 80 °C and 100 °C) by curing it on a rheometer in oscillatory shear mode at 1 Hz. In Fig. 14, the modulus of the complex viscosity $|\eta^*|$ and the loss factor tan δ of the three curing processes are presented as a function of time. The initial value of $|\eta^*|$ was found similar for 80 °C and 100 °C, while a higher value was observed at 20 °C. In accordance with the *in situ* resistivity measurements depicted in Fig. 12, it was observed that the onset of the reaction takes place before and its duration becomes shorter at higher temperatures: at 100 °C (red curves), $|\eta^*|$ starts increasing and stabilizes faster and so does the corresponding peak of tan δ (an indication of the energy dissipation during the reaction). The difference of final $|\eta^*|$ values at different temperatures is correlated to the temperature dependent nature of the mechanical properties of the cured samples.

3.4. Rotational and translational motion of interacting SWCNTs by DEP modeling

The dependence of the polarization factor α^* on the electric field frequency was first explored by means of Eq. (2) with the values from Table 1 and the results are presented in Fig. 15. It can be observed that $\mathrm{Re}[\alpha^*] \sim 265$ is computed for frequencies up to $f \sim 100$ Hz and then the magnitude increases for higher frequencies, reaching a plateau value of $\mathrm{Re}[\alpha^*] \sim 2300$ at approximately $f = 10$ kHz. According to the DEP model, a higher polarization factor indicates higher magnitudes for the electric field-induced torques and forces exerted by the CNT, which would impact in more accelerated dynamics [34,35]. This trend has also been validated by experiments, where authors reported faster and better-aligned structures when the electric field is increased [20,48,49].

From the solution of Eqs. (2) and (3), the temporal evolution of the CNTs angle (black lines) and the CNT-to-CNT separation

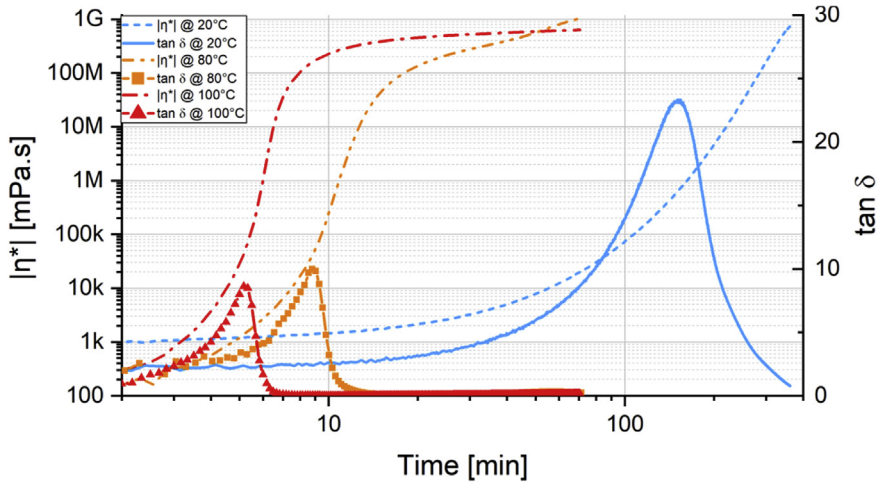

Fig. 14. Modulus of complex viscosity $|\eta^*|$ and loss factor tan δ of SWCNT/epoxy 0.01 wt.% during curing reaction. (A colour version of this figure can be viewed online.)

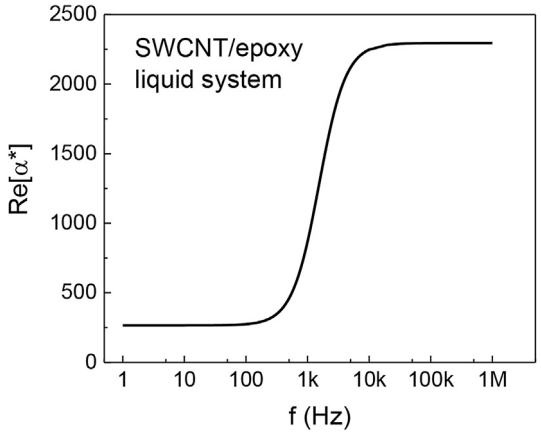

Fig. 15. Real part of the polarization factor α^* (see Eq. (2b)) as a function of the electric field frequency for a SWCNT immersed in liquid epoxy.

distance (β, red lines) is presented in Fig. 16 for cases where the frequency, electric field and viscosity were varied (as in the experiments), in order to explore their influence on the CNTs motion. For all cases, the CNT alignment (i.e. when $\theta \sim 0$) is the first event to be completed and then the CNTs horizontally translate until reaching contact (i.e. when $\beta \sim 0$). For both frequencies, β experiences a sudden decrease (see red lines) which is related to the CNT rotation, i.e. β is lowered as the CNTs rotate towards the alignment condition (see Fig. 16). Once alignment of the CNTs is reached, it can be observed that the translational motion follows a slower rate, experiencing a sudden decrease towards the chained condition ($\beta \sim 0$) once the CNTs are close enough. Fig. 16a shows that faster CNT alignment occurs when the frequency is increased from 50 Hz (black dashed line) to 1 MHz (black solid line). A similar trend is also appreciated for the elapsed time for the CNT-to-CNT chaining (red lines), with shorter elapsed times of chaining when the frequency is increased. As expected from the behavior of the polarization factor in Fig. 15, the dynamic of rotation and translation is accelerated due to the increased DEP-induced torques and forces.

A similar trend regarding the influence of the electric field magnitude (Fig. 16b) and medium viscosity (Fig. 16c) on the alignment and chaining times can be noticed. From Fig. 16b it is seen that the rotational and translational dynamics are accelerated when the electric field magnitude is increased, which can be somehow expected from the quadratic dependence of T_{DEP} on E^2 in Eq. (2a). In addition, higher viscosity promotes a slower rotational and translational motion of the CNT, which can be observed in Fig. 16c. It is important to consider that the DEP model has certain simplified assumptions which may impact in the order of

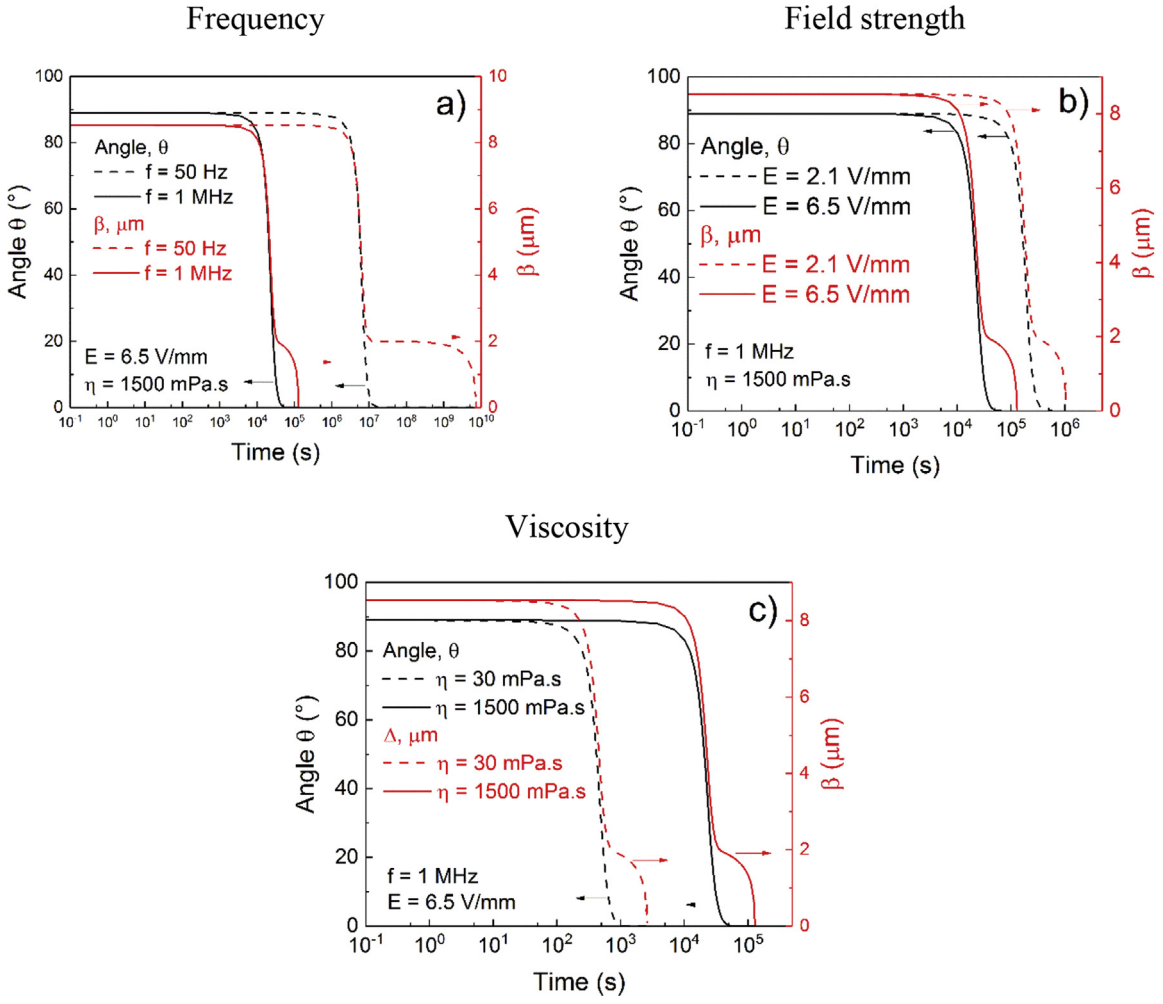

Fig. 16. Rotational angle (left vertical axis) and CNT-to-CNT separation distance (β, right vertical axis) as a function of time for a SWCNT/epoxy system. a) Influence of electric field frequency, b) influence of electric field magnitude, c) influence of medium. (A colour version of this figure can be viewed online.)

Table 2
Relevant material properties and CNT geometry [50].

Material	Electrical resistivity	Diameter	Length
CNT	10^{-4} Ω·m	50 nm	5 μm
Epoxy	10^{6} Ω·m	–	–

magnitude of the predicted times, which may seem very long. For example, CNTs are considered isolated with influence of solely their first neighbor CNT. This fact neglects other type of interactions that would contribute to accelerated processes. Also, no electric field gradients are considered, which also underestimates the effect of DEP-forces promoting CNT motion.

However, despite these assumptions, the main aim of this simple model is to capture specific trends regarding the influence of experimental parameters associated with the experiments. The connection of the trends predicted by the DEP model with the experimental results will be properly discussed in following sections.

3.5. *Effects of the minimum distance between CNTs on the composite bulk conductivity*

The FE methodology described in Section 4 is now used to investigate the effect of infinitesimal changes of the minimum contact separation between CNTs within the polymer matrix, and its relation to the measured improvements in conductivity. We will consider a test case based on the CNT dispersion in epoxy as investigated in Refs. [40,50]. CNT dimensions and properties considered by Hu et al. [50] are presented in Table 2. As before, we consider a nanotube resistivity $\rho_{CNT} = 1/\sigma_{CNT}$ of 10^{-4} Ω·m, and an epoxy (very high) resistivity of 10^{6} Ω·m. For the tunneling junctions, a relative permittivity of 3.98 (representative of epoxy) and a work fraction of 4.95 eV [51] are used.

To allow generalization to any CNT-epoxy system, results are presented in adimensional form (similar to the dimensional analysis presented in [52]). According to the percolation theory [53], the composite conductivity around percolation is proportional to $(\phi/\phi_c - 1)^t$, where ϕ and ϕ_c are the CNT concentration and percolation threshold, respectively, and t is the power law exponent. Therefore, the composite homogenized resistivity $\overline{\rho}$ adimensionalized by the CNT resistivity is presented against the concentration ratio ϕ/ϕ_c.

For this system, the critical percolation threshold is found around a volume fraction of 0.68%, agreeing with the prediction obtained by the excluded volume theory [40,54]. Results are presented for a converged RVE size of $L_{RVE} = 2 \times L_{CNT}$ and results are averaged over 20 realizations and the 3 Cartesian directions. The effect of the minimum distance between CNTs is studied by changing d_{min} varying from the van der Waals distance of 0.34 nm up to 1.0 nm, and the resulting composite conductivity is presented in Fig. 17.

All curves represented in Fig. 17 show the typical response of a percolation problem [10], departing from the matrix conductivity at null concentration and rapidly decreasing in resistivity (or increasing conductivity) with the CNT concentration around the percolation threshold ϕ_c. However, the decrease in resistivity around the percolation threshold becomes less abrupt for higher values of d_{min}. Since the tunneling resistance grows exponentially with the spacing between nanotubes [55], an increase in d_{min} results in much less conductive junctions. Furthermore, the difference between the curves becomes less evident for very low and high CNT concentrations. This is due to the fact that the formation of conductive paths is the dominant conductivity mechanism in these regions, while the relative contribution of the junction resistance is more significant around the percolation, where only a few conductive pathways exist [58].

The ratios between these conductivities and the one for the minimum considered ($d_{min} = 0.34$) are reproduced in Fig. 18, illustrating the potential increase in conductivity resulting from a decrease in nanotube separation. Comparing the conductivity of the two extremes $d_{min} = 0.34$ and $d_{min} = 1.00$, their ratio is maximum around 90% above the critical concentration (1.90 wt.%) with a value of approximately 7×10^{3}. For the highest analyzed concentration, this ratio decreases to 1.25.

These observations suggest that altering the processing method in a fashion that can bring dispersed CNTs closer together will have a much more significant effect on the resistivity change near the percolation region. At the same time, the potential improvement in conductivity and its sensitivity to CNT concentration follows the trends observed experimentally when curing under an electric field, suggesting that this processing method alters the CNT network by influencing the CNT-CNT contact points.

4. Discussion

To evaluate the morphology of SWCNT networks, SEM was used to investigate the nanocomposite samples produced. Fig. 19 shows the SWCNTs in their as-received powder form (a) and a cryo-

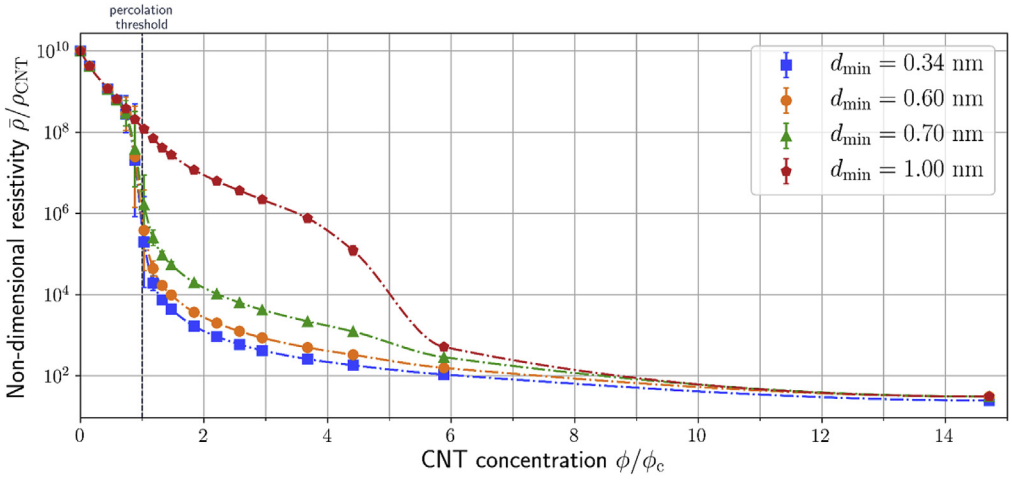

Fig. 17. Homogenized electrical resistivity as function of the CNT concentration divided by its percolation threshold, considering different values of the minimum distance between CNTs. Bars represent the standard deviation. (A colour version of this figure can be viewed online.)

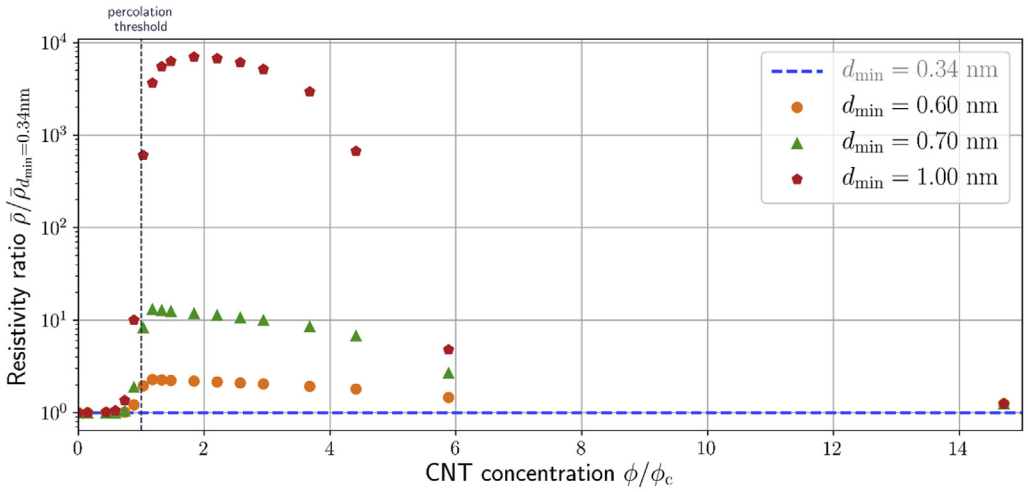

Fig. 18. Ratio of the homogenized resistivity with respect to the minimum distance $d_{\min} = 0.34$ nm. (A colour version of this figure can be viewed online.)

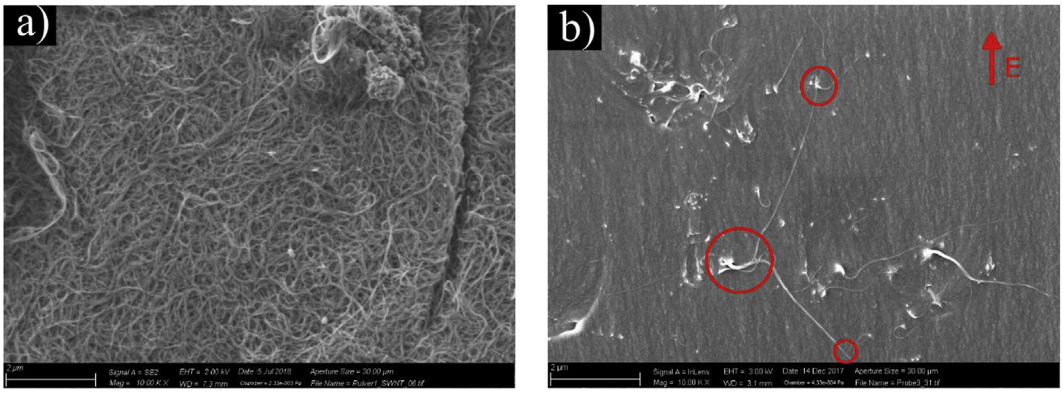

Fig. 19. SEM images of a) the pristine SWCNT powder and b) cryo-fractured SWCNT/epoxy 0.01 wt% specimen produced under effect of electric field (direction indicated by red arrow). Red circles indicate possible bridging point between adjacent SWCNTs. (A colour version of this figure can be viewed online.)

fractured surface of a SWCNT/epoxy 0.01 wt.% specimen cured under the effect of an AC field (b). Thin and long individual structures can be clearly seen in Fig. 19b, confirming the SWCNTs dispersion by the three-roll mill technique and subsequent composite fabrication process. According to transmission electron microscope observations of the SWCNTs used [56], it is generally expected that the individual structures are actually strands (microcrystals) of SWCNTs with a thickness of around 20 nm as a consequence of the manufacturing process. As it is possible to observe in Fig. 19, these strands display a wavy and flexible shape quite distinct from the ideal conception of rigid tubes at the macro scale. Moreover, on the samples treated with an electric field, the SWCNTs do not appear to present a defined preferential orientation along the field direction (indicated on the top right-hand side corner), despite the clear decay in electrical resistivity measured. It should be noted that these images represent only a reduced two-dimensional perspective of the bulk material and that the chance of getting representative results in exactly the fracture surface is extremely low. Nevertheless, one can presume to recognize some contact points between neighboring particles (marked in red). An improvement on the electrical conductivity of the final bulk material could be thereby explained by changes in these CNT-to-CNT contacts.

Both the *ex situ* and *in situ* resistivity measurements to SWCNT/epoxy samples produced under the influence of electric fields have shown a clear dependency on the field parameters. Simulations based on the DEP theory allowed for investigating theoretical trends that help explaining those experimental results, namely the effects of the field frequency and electric field strength, together with the viscosity of the liquid system.

Following the experiments depicted in Fig. 7, while DC fields did not lead to much decrease in the electrical resistivity of the final composites, AC electric fields promoted an improvement of up to one order of magnitude. Such enhanced networks could be interpreted, based on the illustration presented in Fig. 20, as follows: due to the electric field, polarization of the SWCNTs takes place, leading to interactions with the field and the other nanotubes, according to DEP theory. When these nanotubes get close enough to the electrodes to allow the transfer of charges, they discharge and adsorb onto them. Then, the tips of the nanotubes connected to the electrodes become sources of high field strengths, constituting points for adsorption of more filler particles. The subsequent addition of more carbon nanotubes ultimately leads to a network structure extending from one electrode and reaching the other, providing conductive pathways throughout the specimen.

When DC electric fields were applied, however, no significant decrease of the electrical resistivity was observed (Fig. 7). This can be explained by migration of charged nanotubes towards the electrodes under electrophoresis. Charging of the SWCNTs might be attributed to electrostatic interactions arising in the mixing process

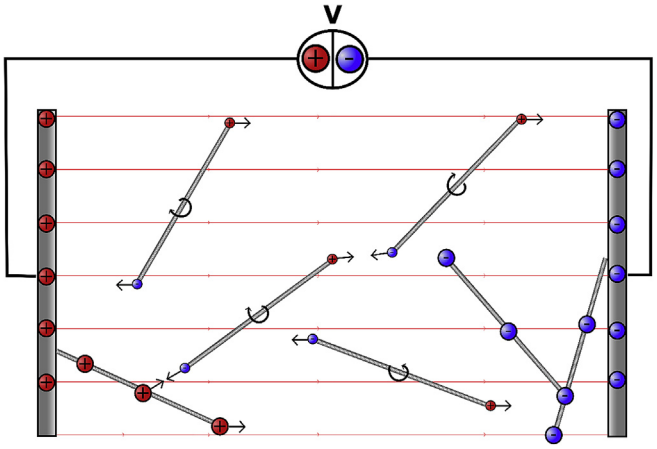

Fig. 20. Randomly dispersed CNTs become polarized and orient under dielectrophoretic forces and torque, interact due to attractive and repulsive Coulomb forces, and assemble in conductive chains. (A colour version of this figure can be viewed online.)

or due to the presence of negative surface charges on the nanotubes in an epoxy matrix. This effect was also observed in [23], with the nanotubes migrating towards the anode.

Furthermore, a clear dependency on the frequency was verified, but such effect stabilized above ca. 50 kHz (Fig. 7), i.e. for the frequencies tested above this value (500 kHz, 1 MHz, 10 MHz) the electrical resistivity stayed in the same range. One way of interpreting these results using DEP theory is to analyze the development of the polarization factor α^* with the electric field frequency. In fact, according to equation (2a), the DEP-induced torque on the CNTs is directly proportional to $\mathrm{Re}[\alpha^*]$, meaning the higher $\mathrm{Re}[\alpha^*]$, the stronger the momentum on the CNTs causing them to reorient. Interestingly, from the DEP model of this SWCNT/epoxy system, $\mathrm{Re}[\alpha^*]$ increases for higher frequencies up until a plateau at around 10 kHz (Fig. 15). This implies that the frequency contribution for the DEP torque (and hence for the conductive network formation) is maximized at this frequency range, thereby providing a possible explanation for the frequency dependency of resistivity improvement observable on Fig. 7. From Figs. 6 and 11, the higher the electric field strength (E) applied (or voltage) the lower the resistivity of the SWCNT/epoxy composites produced. This is related to dependency of the DEP-induced torque (T_{DEP}) on E^2 (Eq. (2a)) and this effect is verified by the DEP simulations where E was varied according to the experimental setup. In fact, increasing the field strength from 2.1 kV/m to 6.5 kV/m in the modeling scenario of the two interacting CNTs leads to a decrease of the alignment time of around one order of magnitude (Fig. 16b).

The third parameter investigated using the DEP model was the viscosity of the medium. Fig. 16c presents the CNT angle and chaining for the viscosities of 30 and 1500 mPa·s. As predicted, at higher viscosity the rotational and translational motion of the CNT becomes slower. This can be of critical importance given the fact that the system under investigation is a reactive one, and so there is only a limited amount of time for a rearrangement of the CNTs to take place, as evident by the rheological behavior displayed in Fig. 14. Indeed, accounting for the curing dynamics and the onset of the reaction only, lower curing temperature would allow more time for the electric field to influence the CNTs and hence lower electrical resistivity of the final composite. Nonetheless, despite faster reaction times, higher curing temperatures have shown to promote lower electrical resistivity, as distinctly observed in the *in situ* resistivity curves plotted in Fig. 12. This can be noticed also for the difference between the samples cured at 80 °C and 100 °C. Even though the reaction is faster at the higher temperature – tan δ peak takes place around 4 min before (Fig. 14) – i.e. the time window for the electric field to act reduces from 9 min to 5 min (almost 50%) – the final resistivity values are still slightly lower for 100 °C (Figs. 8 and 12). One likely explanation for this phenomenon is the decreasing behavior of the viscosity with increased temperature, as depicted in Fig. 13. Another possibility is the temperature dependency of Brownian motion, which also plays a role in particle dynamics [23,30,31,36,37,48].

It is essential to realize that for reducing the electrical resistivity of the SWCNT/epoxy composites two experimental instruments were applied: the curing temperature and the electric field. As a matter of fact, Fig. 8 shows that a decay in the resistivity of one order of magnitude was achieved solely through increase of the curing temperature. This is thought to be related to the viscosity decrease with temperature, allowing for particle mobility and therefore van der Waals and π-π interactions [28,30,34]. In general, low viscosity systems promote more CNT-CNT connections due to the particle interactions and enhanced CNT mobilities, rendering lower resistivities and percolation thresholds on such systems [57]. An additional improvement of the same magnitude is thereafter attained by exposing the SWCNT/epoxy to AC electric fields during curing. This reveals two independent phenomena which, when combined, allow for a two order of magnitude decrease in electrical resistivity for composites with the same concentration of conductive nanoparticles.

One additional possibility has yet to be considered: the electric field resulting in resin heating. Indeed, a temperature difference of 15 °C was verified between the samples cured at RT with and without electric field. To exclude the hypothesis that the resistivity decay in the samples cured under electric field is related only to temperature, further samples were cured at 140 °C. If the resistivity decrease is merely a temperature effect, then the resistivity of both samples with and without field should be more similar for a temperature high enough to prevail over the heating generated from the electric field. However, the samples cured under an electric field and curing temperature of 140 °C also show a resistivity one order of magnitude lower than those without field. This fact gives additional confidence that the decrease of resistivity measured in this investigation comes from two independent effects: electric field and temperature.

In a second stage, to validate the assumption that the decreased resistivity was due to an improvement of the contact between the CNTs, FE simulations of CNT networks in a matrix were performed and their electrical resistivity was computed for several configurations (contact distances) and concentrations. By investigating the impact of infinitesimal changes on the minimum contact distance between CNTs, presented in Fig. 17, one can conclude that a variation from 0.34 nm to 0.70 nm can promote a decrease of one order of magnitude on the overall bulk resistivity. From 0.70 nm to 1 nm, the change is even more remarkable – between two and three orders of magnitude. In other words, a sub-nanometer change on the contact points separating the CNTs can lead to a bulk effect of up to three orders of magnitude on the electrical properties. This provides a possible interpretation for the separate and combined effects of the curing temperature (and hence viscosity) and electric field in Fig. 8: both impact the distance between the individual particles (i.e. the contact points) leading to measurable bulk effects.

For instance, curing the SWCNT/epoxy composites under the effect of AC electric fields at room temperature (second blue column in Fig. 8) promotes a final bulk resistivity similar to the composites without electric field but cured at higher temperatures (left orange and red columns), with a larger dispersion of results indicated by the error bar. This could reflect a comparable average contact distance. Yet, for the samples produced with both AC electric fields and higher temperature (red orange and red

columns), the chaining distance is further decreased at the sub-nanometer level, rendering an additional improvement of one order of magnitude on the resistivity.

FE simulations allowed to explore the impact of varying the inter-nanotube separation distance at different CNT concentrations. This is related with the relative importance of the different conduction mechanisms, dominated by conductive pathways and conductivity between contacting CNTs, at different concentrations. According to the percolation theory [53], there is a minimum concentration threshold that enables the flow of electrons throughout the material. Below this concentration, the material is electrically insulating, since there are no pathways for current to pass through. Then, at the percolation concentration, an abrupt increase of many orders of magnitude in the conductivity takes place. Around this concentration, only a few conductive paths exist and therefore the influence of the contact resistance is more significant. Far above the critical concentration, adding more CNTs contributes to more parallel conductive paths, and therefore these pathways become the dominant conductivity mechanism [58]. Nonetheless, it should be noted that this theory does not take the processing method used to produce the composite into account.

As displayed in Fig. 9, even though specimens with 0.01 wt.% SWCNTs have shown a decrease of one order of magnitude solely due to the effect of the electric field, such behavior was not verified for the concentrations of 0.005 wt.% and 0.1 wt.%. Naturally, the questions arise: can the electrical resistivity of such composites be influenced even if the particle network is still not percolated? Moreover, if there is already a network with enough contacts for electricity to flow (i.e. above the percolation threshold), can we still improve its conductivity by promoting further chaining points? According to the FE simulations of conductive networks for different concentrations, presented in Fig. 18, there is in fact a lower as well as an upper concentration limit where a change of the contacting distances between the CNTs has a much less pronounced effect on the bulk resistivity. This means that if the particle amount is too low, as it was the case for the 0.005 wt.% samples produced, improving the contact points between the particles still brings no significant improvement. On the other hand, for higher concentrations above percolation, as for the 0.1 wt.% SWCNT/epoxy specimens, the particle network has already so many parallel conductive pathways, even without using electric fields, that further changes do not impact much the final resistivity.

It should be emphasized that this modeling approach was meant to identify tendencies on the electrical properties of the bulk composites for changes on the above-mentioned parameters. The aspect ratio of the CNTs modeled with FE (100) was considerably shorter than that of the CNTs used in experiments (2777), due the limiting computation effort of the simulations. Regardless, the results are presented in non-dimensional form to ease the generalization of these conclusions.

5. Conclusions

The influence of applying an electric field during the curing process of SWCNT/epoxy nanocomposites was investigated. In terms of electrical resistivity, the advantage of such process was successfully verified, with a reduction of up to one order of magnitude. It is suggested that this improvement in the electrical properties is due to a field induced orientation and assembly of the nanotubes into an enhanced conductive network. For the concentration of 0.01 wt%, a decrease of the electrical resistivity was observed for composites produced with increased field strength and frequency. Increasing the curing temperature from RT to 100 °C also led to a reduction in the electrical resistivity of one order of magnitude.

Such field effects were studied using a classical mechanics model based on dielectrophoresis to help interpreting the experimental results, revealing an excellent agreement with the observed tendencies. Furthermore, FE simulations of CNT networks in epoxy were performed to investigate the effect of the minimum inter-nanotube distance on the bulk conductivity, providing a possible explication for the conductivity increase found for different curing temperatures and electric fields. These simulations demonstrate that the possibility of affecting the resistivity, by influencing the contact points between the particles, is much more significant for a concentration range around the percolation than for lower and higher concentrations.

Overall, this technique highlights promising results for enhancing the electrical conductivity of polymer composites with carbon-based nanoparticles by influencing the particle nanostructure during the processing step. Such a technology would enable lowering the CNT content required for attaining similar electrical properties, thereby allowing the tailoring and production of more cost-effective nanocomposites with a wide range of industrial applications such as battery, sensing, and heat management technologies. Further research in this topic will aim at understanding the impact of the type of nanoparticles employed, stronger electric fields for lower particle concentrations, the limitations in terms of matrix viscosity, as well as the development of simulation tools capable of fully reproducing the processing methods.

Acknowledgments

This research has received funding from the European Union's Horizon 2020 research and innovation program under the Marie Skłodowska-Curie Grant Agreement no. 642890 (TheLink, www.thelink-project.eu). AI Oliva-Avilés acknowledges the support of the "Fondo Sectorial de Investigación para la Educación" through the SEP-CONACYT grant No. 235905. The authors also wish to thank Markus Schönwald, Ulrich Förter-Barth and Birgit Eickershoff of the Fraunhofer Institute for Chemical Technology (ICT), for the contributions to the development of the experimental setups, the rheological measurements and the SEM investigations, respectively.

References

[1] R.A. Matula, Electrical-resistivity of copper, gold, palladium, and silver, J. Phys. Chem. Ref. Data 8 (4) (1979) 1147–1298.
[2] D.C. Giancoli, Physics: Principles with Applications, Prentice-Hall, 1995.
[3] G. Kaur, R. Adhikari, P. Cass, M. Bown, P. Gunatillake, Electrically conductive polymers and composites for biomedical applications, RSC Adv. 5 (47) (2015) 37553–37567.
[4] R. Yeetsorn, M.W. Fowler, C. Tzoganakis, A Review of Thermoplastic Composites for Bipolar Plate Materials in PEM Fuel Cells, Nanocomposites with Unique Properties and Applications in Medicine and Industry, 2011.
[5] A.R. Boccaccini, J. Cho, J.A. Roether, B.J.C. Thomas, E.J. Minay, M.S.P. Shaffer, Electrophoretic deposition of carbon nanotubes, Carbon 44 (15) (2006) 3149–3160.
[6] M. Diba, D.W.H. Fam, A.R. Boccaccini, M.S.P. Shaffer, Electrophoretic deposition of graphene-related materials: a review of the fundamentals, Prog. Mater. Sci. 82 (2016) 83–117.
[7] Y.C. Lan, Y. Wang, Z.F. Ren, Physics and applications of aligned carbon nanotubes, Adv. Phys. 60 (4) (2011) 553–678.
[8] Z. Li, K.S. Moon, Y.G. Yao, K. Hansen, K. Watkins, L. Morato, et al., Carbon nanotube/polymer nanocomposites: sensing the thermal aging conditions of electrical insulation components, Carbon 65 (2013) 71–79.
[9] F. Inam, B.R. Bhat, N. Luhyna, T. Vo, Comparison of structural health assessment capabilities in epoxy - carbon black and epoxy - carbon nanotube nanocomposites, Express Polym. Lett. 8 (1) (2014) 55–61.
[10] M. Sahimi, Applications of Percolation Theory, Taylor \& Francis, 2003.
[11] W. Bauhofer, J.Z. Kovacs, A review and analysis of electrical percolation in carbon nanotube polymer composites, Compos. Sci. Technol. 69 (10) (2009) 1486–1498.
[12] I. Alig, P. Pötschke, D. Lellinger, T. Skipa, S. Pegel, G.R. Kasaliwal, et al., Establishment, morphology and properties of carbon nanotube networks in polymer melts, Polymer 53 (1) (2012) 4–28.

[13] M.T. Muller, B. Krause, B. Kretzschmar, P. Potschke, Influence of feeding conditions in twin-screw extrusion of PP/MWCNT composites on electrical and mechanical properties, Compos. Sci. Technol. 71 (13) (2011) 1535–1542.
[14] G. Olowojoba, S. Sathyanarayana, B. Caglar, B. Kiss-Pataki, I. Mikonsaari, C. Hübner, et al., Influence of process parameters on the morphology, rheological and dielectric properties of three-roll-milled multiwalled carbon nanotube/epoxy suspensions, Polymer 54 (1) (2013) 188–198.
[15] G. Olowojoba, S. Sathyanarayana, B. Caglar, I. Mikonsaari, C. Hübner, P. Elsner, Influence of processing temperature, carbon nanotube agglomerate bulk density and functionalization on the dielectric and morphological properties of carbon nanotube/epoxy suspensions, in: Proceedings of the PPS 29th Annual Meeting Nürnberg, Germany, 2013.
[16] K. Yamamoto, S. Akita, Y. Nakayama, Orientation of carbon nanotubes using electrophoresis, Jpn. J. Appl. Phys. 2 (35) (1996) L917–L918, 7b.
[17] K. Yamamoto, S. Akita, Y. Nakayama, Orientation and purification of carbon nanotubes using ac electrophoresis, J. Phys. D Appl. Phys. 31 (8) (1998) L34–L36.
[18] X.Q. Chen, T. Saito, H. Yamada, K. Matsushige, Aligning single-wall carbon nanotubes with an alternating-current electric field, Appl. Phys. Lett. 78 (23) (2001) 3714–3716.
[19] R. Krupke, F. Hennrich, H.B. Weber, D. Beckmann, O. Hampe, S. Malik, et al., Contacting single bundles of carbon nanotubes with alternating electric fields, Appl. Phys. Mater. Sci. Process 76 (3) (2003) 397–400.
[20] M.S. Kumar, T.H. Kim, S.H. Lee, S.M. Song, J.W. Yang, K.S. Nahm, et al., Influence of electric field type on the assembly of single walled carbon nanotubes, Chem. Phys. Lett. 383 (3–4) (2004) 235–239.
[21] J.Q. Li, Q. Zhang, N. Peng, Q. Zhu, Manipulation of carbon nanotubes using AC dielectrophoresis, Appl. Phys. Lett. 86 (15) (2005).
[22] Z. Chen, Y.L. Yang, F. Chen, Q. Qing, Z.Y. Wu, Z.F. Liu, Controllable interconnection of single-walled carbon nanotubes under ac electric field, J. Phys. Chem. B 109 (23) (2005) 11420–11423.
[23] C.A. Martin, J.K.W. Sandler, A.H. Windle, M.K. Schwarz, W. Bauhofer, K. Schulte, et al., Electric field-induced aligned multi-wall carbon nanotube networks in epoxy composites, Polymer 46 (3) (2005) 877–886.
[24] C. Park, J. Wilkinson, S. Banda, Z. Ounaies, K.E. Wise, G. Sauti, et al., Aligned single-wall carbon nanotube polymer composites using an electric field, J. Polym. Sci., Polym. Phys. Ed. 44 (12) (2006) 1751–1762.
[25] L. Valentini, S.B. Bon, J.M. Kenny, Anisotropic electrical transport properties of aligned carbon nanotube/PMMA films obtained by electric-field-assisted thermal annealing, Macromol. Mater. Eng. 293 (11) (2008) 867–871.
[26] Y.F. Zhu, C. Ma, W. Zhang, R.P. Zhang, N. Koratkar, J. Liang, Alignment of multiwalled carbon nanotubes in bulk epoxy composites via electric field, J. Appl. Phys. 105 (5) (2009).
[27] A.I. Oliva-Aviles, F. Aviles, V. Sosa, Electrical and piezoresistive properties of multi-walled carbon nanotube/polymer composite films aligned by an electric field, Carbon 49 (9) (2011) 2989–2997.
[28] A.I. Oliva-Aviles, F. Aviles, V. Sosa, A.I. Oliva, F. Gamboa, Dynamics of carbon nanotube alignment by electric fields, Nanotechnology 23 (46) (2012).
[29] M. Felisberto, A. Arias-Duran, J.A. Ramos, I. Mondragon, R. Candal, S. Goyanes, et al., Influence of filler alignment in the mechanical and electrical properties of carbon nanotubes/epoxy nanocomposites, Physica B 407 (16) (2012) 3181–3183.
[30] M. Monti, M. Natali, L. Torre, J.M. Kenny, The alignment of single walled carbon nanotubes in an epoxy resin by applying a DC electric field, Carbon 50 (7) (2012) 2453–2464.
[31] O. Osazuwa, M. Kontopoulou, P. Xiang, Z.B. Ye, A. Docoslis, Electrically conducting polyolefin composites containing electric field-aligned multiwall carbon nanotube structures: the effects of process parameters and filler loading, Carbon 72 (2014) 89–99.
[32] E.M. Remillard, Q.Y. Zhang, S. Sosina, Z. Branson, T. Dasgupta, C.D. Vecitis, Electric-field alignment of aqueous multi-walled carbon nanotubes on microporous substrates, Carbon 100 (2016) 578–589.
[33] OCSiAl, TUBALL™ Technical Info, 2018. http://tuball.com/en/about-tuball. (Accessed 30 December 2018).
[34] A.I. Oliva-Aviles, F. Aviles, V. Sosa, G.D. Seidel, Dielectrophoretic modeling of the dynamic carbon nanotube network formation in viscous media under alternating current electric fields, Carbon 69 (2014) 342–354.
[35] A.I. Oliva-Aviles, V.V. Zozulya, F. Gamboa, E. Aviles, Dynamic evolution of interacting carbon nanotubes suspended in a fluid using a dielectrophoretic framework, Physica 83 (2016) 7–21.
[36] T.B. Jones, T.B. Jones, Electromechanics of Particles, Cambridge University Press, 2005.
[37] H. Morgan, N.G. Green, AC Electrokinetics: Colloids and Nanoparticles, Research Studies Press, 2003.
[38] T.W. Ebbesen, H.J. Lezec, H. Hiura, J.W. Bennett, H.F. Ghaemi, T. Thio, Electrical conductivity of individual carbon nanotubes, Nature 382 (6586) (1996) 54–56.
[39] C. Laurent, E. Flahaut, A. Peigney, The weight and density of carbon nanotubes versus the number of walls and diameter, Carbon 48 (10) (2010) 2994–2996.
[40] M.A.S. Matos, V.L. Tagarielli, P.M. Baiz-Villafranca, S.T. Pinho, Predictions of the electro-mechanical response of conductive CNT-polymer composites, J. Mech. Phys. Solids 114 (2018) 84–96.
[41] L.A. Girifalco, M. Hodak, R.S. Lee, Carbon nanotubes, buckyballs, ropes, and a universal graphitic potential, Phys. Rev. B 62 (19) (2000) 13104–13110.
[42] D.S. Simulia, Abaqus 2017 Documentation, 2017.
[43] J.N. Reddy, An Introduction to the Finite Element Method, McGraw-Hill, 2006.
[44] D.S. Simulia, Abaqus User Subroutines Guide, 2017.
[45] M. Di Ventra, Electrical Transport in Nanoscale Systems, Cambridge University Press, 2008.
[46] J.G. Simmons, Generalized thermal J-V characteristic for the electric tunnel effect, J. Appl. Phys. 35 (9) (1964) 2655–2658.
[47] J. Wang, S. Yu, S. Luo, B. Chu, R. Sun, C.-P. Wong, Investigation of nonlinear I–V behavior of CNTs filled polymer composites, Mater. Sci. Eng., B 206 (2016) 55–60.
[48] R.J. Castellano, C. Akin, G. Giraldo, S. Kim, F. Fornasiero, J.W. Shan, Electrokinetics of scalable, electric-field-assisted fabrication of vertically aligned carbon-nanotube/polymer composites, J. Appl. Phys. 117 (21) (2015) 214306.
[49] B.D. Smith, T.S. Mayer, C.D. Keating, Deterministic assembly of functional nanostructures using nonuniform electric fields, Annu. Rev. Phys. Chem. 63 (2012) 241–263.
[50] N. Hu, Y. Karube, C. Yan, Z. Masuda, H. Fukunaga, Tunneling effect in a polymer/carbon nanotube nanocomposite strain sensor, Acta Mater. 56 (13) (2008) 2929–2936.
[51] M. Shiraishi, M. Ata, Work function of carbon nanotubes, Carbon 39 (12) (2001) 1913–1917.
[52] M.A.S. Matos, S.T. Pinho, V.L. Tagarielli, Predictions of the electrical conductivity of composites of polymers and carbon nanotubes by an artificial neural network, Scripta Mater. 166 (2019) 117–121.
[53] D. Stauffer, A. Aharony, Introduction to Percolation Theory, Taylor & Francis, 2003.
[54] I. Balberg, C.H. Anderson, S. Alexander, N. Wagner, Excluded volume and its relation to the onset of percolation, Phys. Rev. B 30 (7) (1984) 3933–3943.
[55] J.G. Simmons, Generalized formula for the electric tunnel effect between similar electrodes separated by a thin insulating film, J. Appl. Phys. 34 (6) (1963) 1793.
[56] A.V. Krestinin, N.N. Dremova, E.I. Knerel'man, L.N. Blinova, V.G. Zhigalina, N.A. Kiselev, Characterization of SWCNT products manufactured in Russia and the prospects for their industrial application, Nanotechnol Russ. 10 (7–8) (2015) 537–548.
[57] R. Socher, B. Krause, M.T. Müller, R. Boldt, P. Pötschke, The influence of matrix viscosity on MWCNT dispersion and electrical properties in different thermoplastic nanocomposites, Polymer 53 (2) (2012) 495–504.
[58] G.D. Seidel, D.C. Lagoudas, Micromechanical analysis of the effective elastic properties of carbon nanotube reinforced composites, Mech. Mater. 38 (8–10) (2006) 884–907.